Chimia 55 (2001) 517–522

ISSN 0009–4293

Order and Phase Separation in Alloys

Gernot Kostorz* and Bernd Schönfeld

Abstract: In an initially homogeneous alloy quenched from high temperature, local ordering and/or phase separation may occur on the way towards thermodynamic equilibrium at a lower temperature. Some of the related diffuse scattering effects, including those around the primary beam (small-angle scattering), are presented, and some recent results of X-ray and neutron scattering studies of short-range order and decomposition in some alloys are discussed.

Keywords: Alloys · Diffuse scattering · Ordering of alloys · Phase separation · Small-angle scattering

1. Introduction

Ever since X-ray diffraction in crystals was demonstrated [1], standard crystallographic methods have been developed and used to obtain average structural information (*i.e.* on the position of atoms within the unit cell) on many crystalline materials on the basis of Bragg's law, *i.e.* from measurements of Bragg peaks of powder or single-crystalline samples. Neutron diffraction is a little more recent [2]. While X-rays are scattered by the electrons in the sample and are thus 'element-specific', neutrons are scattered by nuclei (and also, through the interaction with their magnetic moment, by local variations of the magnetic induction) and are 'nucleus-specific'. It has also been known for a long time that any random arrangement of two or more scattering species on an average lattice will introduce some diffuse scattering intensity between the Bragg peaks – so-called (monotonic) Laue scattering. (In practice, thermal diffuse scattering may be more prominent in the case of X-rays. For neutrons, nuclear spins and mixtures of isotopes with different scattering powers lead to 'incoherent scattering' as an additional background.) Any deviation from randomness in the occupation of lattice sites and attendant changes in interatomic distances will modulate the diffuse scattering accordingly, and it is this (coherent elastic) diffuse scattering that is most important for materials science, since the microstructural features that are at the origin of such scattering must be known in order to understand many macroscopic properties and property changes.

According to the Fourier theorem, local inhomogeneities of very small (atomic scale) extent in real space will cause coherent scattering essentially everywhere in reciprocal space, while larger inhomogeneities will lead to larger scattering contributions close to the transmitted beam and near Bragg peaks. Schematically, the difference of coherent scattering of a real alloy crystal and of an ideal, chemically pure crystal is illustrated in Fig. 1. Diffuse X-ray scattering is more commonly used than neutron scattering and is presently receiving increased attention owing to the availability of powerful and highly resolving instruments at synchrotron radiation sources, but there are some limitations owing to background contributions from Compton scattering, thermal diffuse scattering, and, near an absorption edge, resonant Raman scattering. Truly elastic diffuse scattering may be measured conveniently with thermal or cold neutrons, as inelastic scattering may be eliminated (except very close to Bragg peaks) by energy analysis of the scattered neutrons. As for both types of radiation, the scattering by inhomogeneities is usually weak, the kinematic scattering theory is applicable.

The diffuse scattering around the primary beam is called small-angle scattering (SAS). It may be measured in transmission or – surface sensitive – in grazing incidence near the critical angle for total reflection. In the standard transmission experiments, neutrons are advantageous because absorption is low for most materials.

Fig. 1. Scattering (schematic) from a binary alloy crystal (with some short-range order). The Bragg positions of a perfect pure crystal of the solvent species are indicated by the thin vertical lines.

*Correspondence: Prof. Dr. G. Kostorz
ETH Zürich
Institut für Angewandte Physik
CH-8093 Zürich
Tel.: +41 1 633 2133
Fax: +41 1 633 1105
E-Mail: kostorz@iap.phys.ethz.ch

The theory of scattering by real crystals has been treated extensively by Krivoglaz [3], for SAS of X-rays mostly by Guinier and Fournet [4][5] and Porod [6]. These basic treatments may be easily adapted to non-polarized neutrons [7][8]. For magnetic diffuse scattering, see [9][10]. A more detailed comparison of X-rays and neutrons for metallurgical studies may be found in [8], and in the following only some basic features will be summarized. Subsequently, a few recent examples of the authors' current research activities will be given.

2. Short-range Order in Substitutional Solid Solutions

The coherent elastic scattering intensity of any system is proportional to the square of the scattering amplitude $F(\mathbf{Q})$ where $\mathbf{Q} = \mathbf{k}\text{-}\mathbf{k}_0$ is the scattering vector and $\mathbf{k}_0$, $\mathbf{k}$ are the wave vectors of incident and scattered waves. For elastic scattering, $Q = |\mathbf{Q}| = 4\pi\sin\theta/\lambda$ where θ is half the scattering angle and λ is the wavelength of the radiation used. Thus, the properties of any scattering ensemble are contained in the structure function

$$S(\mathbf{Q}) = |F(\mathbf{Q})|^2 \qquad (1)$$

(also called 'structure factor') which must be appropriately averaged over the whole system.

For a perfect monatomic crystal, $F(\mathbf{Q})$ is given by the phase-weighted sum over all individual scattering objects (atoms or nuclei) in the beam, *i.e.*

$$F(\mathbf{Q}) = b\sum_n \exp(-i\mathbf{Q}\cdot\mathbf{R}_n) \qquad (2)$$

where b is the coherent scattering length (including the form factor and the thermal Debye-Waller factor) and the $\mathbf{R}_n$ are the position vectors in the ideal lattice. With Eqn. (2) in (1), one obtains only Bragg scattering, *i.e.* nonvanishing intensities occur only for special values of $\mathbf{Q}$ that correspond to reciprocal lattice vectors $\mathbf{Q}_B$. In an alloy (for simplicity, we discuss only substitutional alloys, *i.e.* only the sites of the average base lattice, but no interstitial sites, may be occupied by the atoms of the components), b will also depend on the site n, and each atom may also be moved by a local displacement $\mathbf{u}_n$ from the average lattice position $\mathbf{R}_n$, *i.e.* the scattering amplitude of the ensemble becomes

$$F(\mathbf{Q}) = \sum_n b_n \exp[-i\mathbf{Q}\cdot(\mathbf{R}_n+\mathbf{u}_n)] \qquad (3)$$

As the translational symmetry is now broken, Eqn. (1) with $F(\mathbf{Q})$ according to Eqn. (3) yields a finite scattering intensity also between Bragg peaks, which is called diffuse scattering.

Deviations from random site occupancy are generally called short-range order (SRO). The simplest case is a binary alloy A-B without any displacements [*i.e.* all $\mathbf{u}_n = 0$ in Eqn. (3)]. For $\mathbf{Q} \neq \mathbf{Q}_B$ the structure function may then be written as

$$S_{SRO}(\mathbf{Q}) = N|c(\mathbf{Q})|^2 |b_B - b_A|^2 \qquad (4)$$

where

$$|c(\mathbf{Q})|^2 = c(1-c)\alpha(\mathbf{Q}) \qquad (5)$$

with c = atomic fraction of B atoms, while

$$\alpha(\mathbf{Q}) = \sum_n \alpha_{no}\exp(-i\mathbf{Q}\cdot\mathbf{R}'_n), \qquad (6)$$

where $\mathbf{R}'_n$ is a distance vector from the site labelled n to an (arbitrary) reference site within the crystal, and the Warren-Cowley short-range order parameters [11] are defined using the conditional probabilities P_n^{ij} of finding an atom of type $j \in \{A,B\}$ at site n if an atom of type $i \in \{A,B\}$ is at the origin;

$$\alpha_n = \frac{P_n^{BB} - c}{1-c} = \frac{c - P_n^{AB}}{c} \qquad (7)$$

Irrespective of the state of order, α_o must always be equal to one. If A and B atoms are randomly distributed, all other α_n will be zero, and Eqn. (4) yields the simple monotonic Laue scattering (it decreases monotonically for X-rays mainly because of the form-factor variation of the atoms; the static and thermal Debye-Waller factors cause only a weak Q dependence remaining for the case of neutron scattering). Measurements of diffuse elastic scattering will thus, if they show any modulations, reveal short-range order. For example, $\alpha_1 < 0$ means preference of AB nearest-neighbour pairs [see Eqn. (7)], and S_{SRO} is enhanced between Bragg peaks. In the opposite case, $\alpha_1 > 0$, there are more BB pairs than expected from a random distribution (clustering), and an enhancement of diffuse scattering is found near Bragg peaks. In practice, not only several higher-order SRO parameters must be taken into account, but also the additional modulations of diffuse scattering due to atomic displacements [$\mathbf{u}_n \neq 0$ in Eqn. (3)]. A careful separation of these two diffuse scattering contributions is therefore necessary. This separation is only feasible with the required precision if single crystals are studied. Fortunately, the two contributions show a different symmetry in reciprocal space. An expansion of the exponential in Eqn. (3) yields different levels of approximation for the displacement scattering, and first- and second-order approximations work quite well as long as the displacements are not too large. Several methods (see [12]) have been developed for this separation.

Reliable SRO parameters obtained from diffuse scattering may subsequently be used to model the short-range ordered state of a crystal on a computer [13]. As an example, Fig. 2 shows the short-range order scattering intensity from a Ag-13.4 at.% Al single crystal. The sample was aged at 673 K for 184 h and subsequently quenched into iced water. The aging tem-

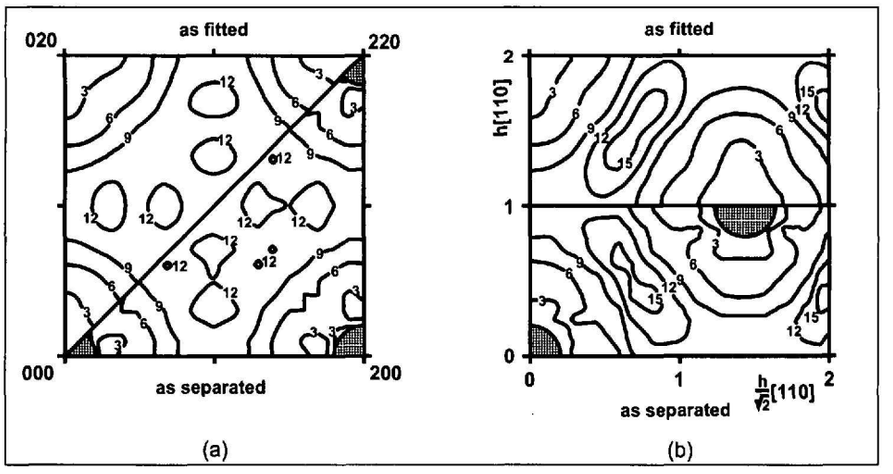

Fig. 2. Short-range order diffuse scattering [lines of equal intensity in 0.1 Laue units; 1 Laue unit = $c(1-c)(\Delta b)^2$] for (a) a (001) and (b) a (110) plane of Ag-13.4 at.% Al. The as-separated data (Georgopoulos-Cohen method) are compared with the pattern recalculated from 27 short-range order parameters obtained by a least-squares fitting of the separated $\alpha(\mathbf{Q})$.

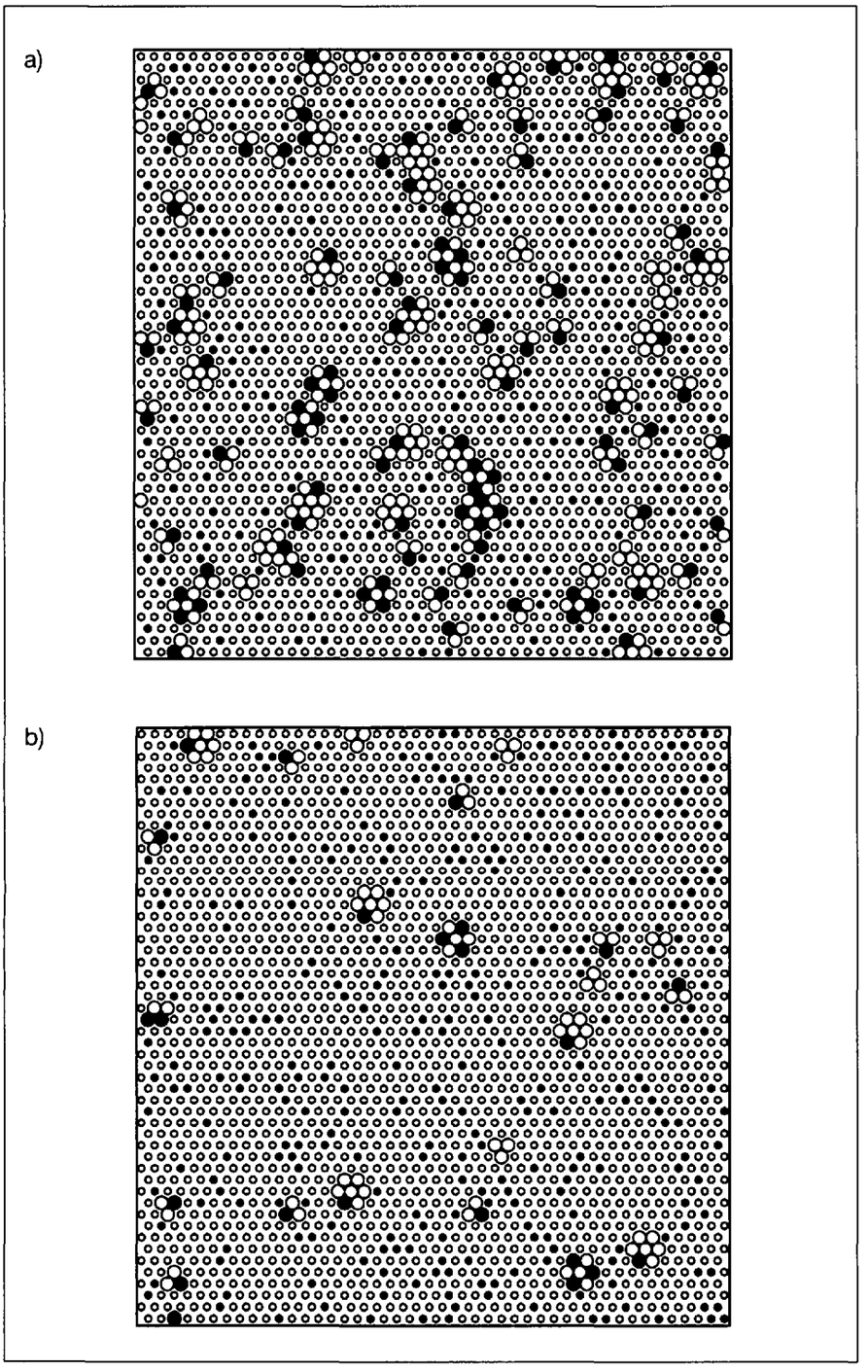

Fig. 3. One of the (111) planes of (a) a modelled short-range-ordered alloy crystal and (b) a crystal with a random arrangement of Ag (open circles) and Al (filled circles). Atoms belonging to the C9 Clapp configuration are shown by enlarged symbols [14].

perature was chosen in the α phase close to the α-μ two-phase region to set up a high degree of short-range order. The diffuse X-ray scattering measurement was performed at room temperature using Mo K_α radiation, and scattering intensities were registered at about 11000 positions under monitor control [14]. To obtain the elastic scattering cross sections from the experimental counts, the scattering was calibrated by comparison with the scattering from polystyrene. Compton scattering and thermal diffuse scattering were calculated and subtracted. Finally, the Georgopoulos-Cohen and the Borie-Sparks methods (see [12]) were used to separate SRO and displacement scattering. Both evaluation schemes yield essentially the same results. Two types of diffuse maxima are observed; an absolute one around $^1/_2\,^1/_2\,^1/_2$, one of the special positions of a f.c.c. crystal, and a local one at $2\mathbf{k}_F$ positions. The latter type arises because of the particularly flat pieces of the Fermi surface along <110> that are spanned by the scattering vector $2\mathbf{k}_F$. The modulation of SRO scattering is weak with respect to the monotonic Laue scattering (1 Laue unit).

Short-range order in real space was visualized on model crystals of 32x32x32 f.c.c. unit cells. To determine the subtle differences, statistically uncorrelated arrangements of alloys with the same composition were also simulated. The modelled crystals were analysed with respect to the 144 distinguishable atomic configurations of the first coordination shell (Clapp configurations [15]). The C9 configuration is found most enhanced in the short-range ordered state in comparison with a random alloy (Fig. 3). This figure also demonstrates that the Clapp configuration C9 (for its nomenclature, see Fig. 4) is uniformly spread in the model alloy, with no indication of any larger ordered cluster. In addition, the Clapp configurations C4 and C5 are also largely enhanced. These three structural elements are all present in Ag_5Al with A_5B structure [16]. *Ab-initio* electronic structure calculations also give the A_5B structure as a possible ground-state structure [17]. Experimentally, no long-range ordered structure is known for the Ag-Al system.

The simulated crystals of the short-range ordered state may be used to calculate effective pair interactions $V_n = \frac{1}{2}(V_n^{AA} + V_n^{BB}) - V_n^{AB}$, if a state of thermodynamic equilibrium is modelled. In the Inverse Monte Carlo method proposed by Gerold and Kern [18], many virtual exchanges of nearest neighbours are introduced to 'test' the equilibrium state, and a large set of corresponding nonlinear equations serves to extract the effective pair interactions for a given number of neighbourhood shells. In this particular case, a set of 14 effective pair interactions is at least required to reproduce short-range order scattering with diffuse maxima at $2\mathbf{k}_F$ and $^1/_2\,^1/_2\,^1/_2$ positions in a subsequent Monte Carlo simulation. For a good reproduction of the short-range order parameters, a set of 18 V_n was finally taken. If one assumes that the V_n do not depend on temperature, the order–disorder transition temperature of Ag_5Al can be estimated by Monte Carlo simulations. With ~135 K this temperature is expectedly low, and is similar to the theoretically derived ordering temperature of ~220 K [17].

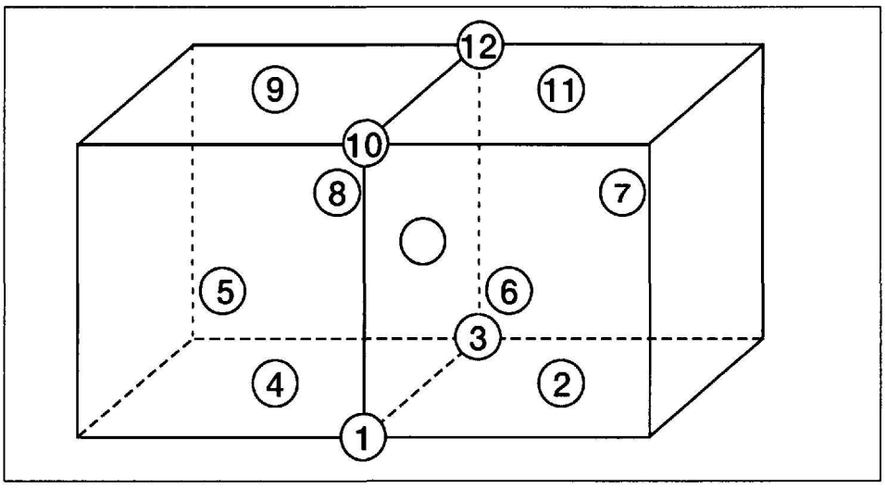

Fig. 4. Nomenclature of nearest-neighbour configurations as introduced by Clapp for the f.c.c. lattice. The configurations found largely enhanced in short-range ordered Ag-rich Ag-Al with respect to a random alloy are C4 (5, 7), C5 (6, 12) and C9 (1, 7, 9). The numbers in brackets denote the sites that are occupied by Al atoms. The other sites in the nearest-neighbour shell as well as the central atom are taken by Ag atoms.

Apart from the possibility of comparing the ground-state energies and stability of different long-range ordered structures, the effective pair interactions are also quite relevant for the deformation behaviour of short-range ordered alloys. When a dislocation in a f.c.c. crystal moves across a (111) plane, it shifts one half-crystal by $\frac{1}{2}$<110> with respect to the other. This changes the number of AA, AB, BB pairs (not only nearest neighbours) across the slip plane, properly weighted by the short-range order parameters. This (static) shift – which can also be repeated for successive motion of dislocations on the same slip plane – changes the configurational energy of the crystal. In obvious correspondence to long-range ordered crystals, this energy may be called diffuse antiphase boundary energy, γ_d [19][20]. It seems to be an important parameter (see [21–23]) in the distinction of 'wavy', distributed glide typically found in pure metals and dilute alloys, and planar glide, *i.e.* a concentration of slip into larger slip steps on fewer planes, characteristic for more concentrated alloys. Fig. 5 shows γ_d (for a large number of slip steps) for three Cu alloys, calculated from the effective pair interactions obtained from diffuse scattering experiments (X-rays for Cu-Al [25], neutrons for Cu-Mn [22] and Cu-Zn [26]). The occurrence of planar slip may be related to an increasing number of dislocations emitted from the same source when γ_d for the first dislocation becomes larger (see [23]).

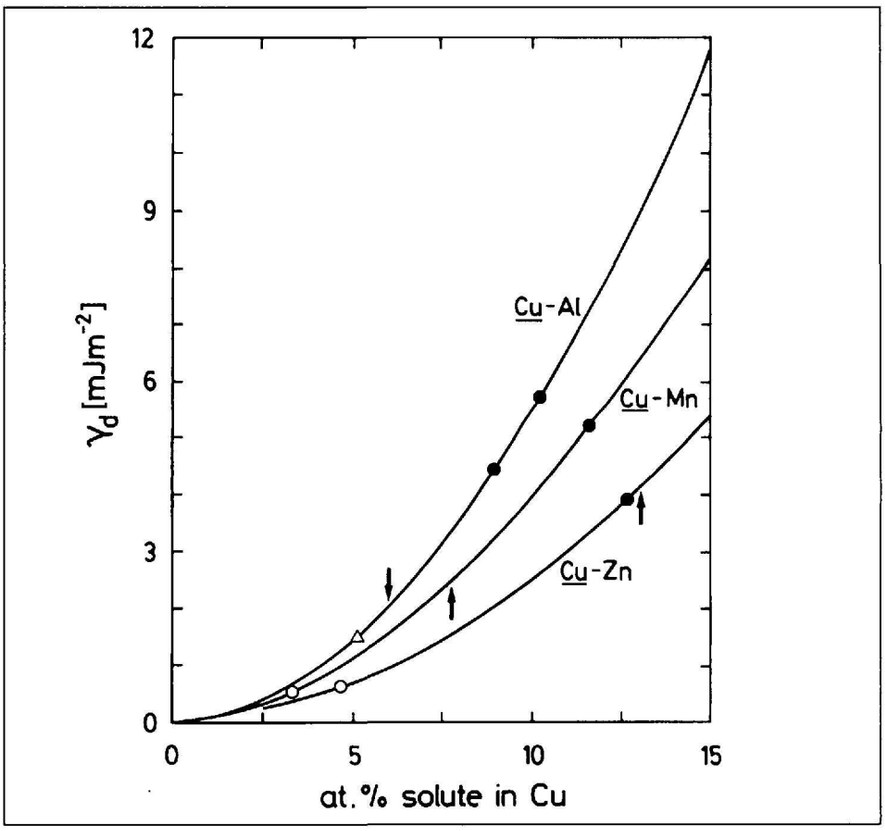

Fig. 5. Diffuse antiphase boundary energy γ_d as a function of solute concentration; continuous lines. Open circles indicate observations of wavy slip, full circles planar glide, and the triangle mixed behaviour. The arrows indicate the wavy → planar transition suggested by Hong and Laird [24] based on a model requiring atomic mobility [22].

So far, alloys with a tendency toward local ordering have been presented. A recent review [27] gives a more detailed assessment of the field. For clustering systems, diffuse scattering measurements are usually more difficult as the relevant scattering occurs close to the Bragg peaks. This requires single crystals of very high perfection and good instrumental resolution. As displacements are systematically larger in decomposing alloys, the separation of SRO and displacement scattering is also more complicated. For the initial stages of decomposition, diffuse scattering measurements have nevertheless contributed considerably to the understanding of alloy behaviour, especially in combination with SAS.

3. Small-angle Scattering

In a limited range of scattering vectors smaller than about π/d where d is the interatomic distance (typically 0.3 nm in condensed matter), the discrete positions of the scattering centres [as in Eqns. (1) and (2)] are no longer resolved. This allows the scattering length distribution to be written as a continuous function, the scattering length density $\rho(\mathbf{r})$, which gives the local average in a volume element $d^3\mathbf{r}$ around the position vector $\mathbf{r}$. The sum in Eqn. (2) may thus be replaced by an integral extending over the sample volume V,

$$F(\mathbf{Q}) = \int_V \rho(\mathbf{r}) \exp(-i\mathbf{Q}\cdot\mathbf{r}) d^3\mathbf{r} \qquad (8)$$

If $\rho(\mathbf{r})$ is constant everywhere in the sample, the scattering intensity will be zero for any accessible $\mathbf{Q} \neq 0$ (for sufficiently large samples), *i.e.* only local deviations of $\rho(\mathbf{r})$ from the macroscopic average $\overline{\rho}$ contribute to the SAS signal. Apart from defects and fluctuations, compositional variations as they occur in decomposing alloys are an important cause for such local variations of scattering length.

3.1. *The Two-phase Model*

The structure function for SAS can be expressed relatively simply, if small particles of a second phase, with a homogeneous scattering-length density ρ_p, are assumed to be embedded in a homogeneous matrix (this could also be a liquid or vacuum) of scattering length density ρ_m. The scattering amplitude, Eqn. (8), then becomes

$$F(\mathbf{Q}) = \int_V (\rho_p - \rho_m)\exp(-i\mathbf{Q}\cdot\mathbf{r})d^3\mathbf{r} \quad (9)$$

The scattering of each individual particle in the ensemble contained in the sample volume V is controlled by the single-particle scattering amplitude

$$F_p(\mathbf{Q}) = V_p^{-1}\int_{V_p} \exp(-i\mathbf{Q}\cdot\mathbf{r})d^3\mathbf{r} \quad (10)$$

where the integration now extends over the particle volume V_p. The amplitude $F_p(\mathbf{Q})$ and the corresponding single-particle scattering function $|F_p(\mathbf{Q})|^2$ can be calculated for many particle shapes (see *e.g.* [4][28]). If there are N particles, all equal and uncorrelated, as in a dilute two-phase system, the scattering function of a sample is

$$S(\mathbf{Q}) = N|F_p(\mathbf{Q})|^2|\rho_p - \rho_m|^2 V_p^2 \quad (11)$$

All the $\mathbf{Q}$ dependence of $S(\mathbf{Q})$ stems from the single-particle scattering function, and the simplest approach in the evaluation of $S(\mathbf{Q})$ is to use Eqn.(11) and knowledge about $|F_p(\mathbf{Q})|^2$ (see *e.g.* [4][6], where a more complete theoretical description of SAS can be found.) In reality, however, there are interparticle interferences in more densely packed particle arrangements, and there are, even if the particles remain self-similar, size distributions that modify the scattering function. For example, a polydisperse uncorrelated ensemble of spheres of radius R with a size distribution n(R) [n(R)dR is the density of particles in the size class (R,R+dR)] leads to

$$S(Q) = |\rho_p - \rho_m|^2 V \int_0^\infty |V_p(R)F_p(Q,R)|^2 n(R)dR \quad (12)$$

The size distribution n(R) can be found from SAS measurements using indirect methods (see *e.g.* [29]). More elaborate, appropriate methods are still being developed for nonspherical particles and systems with interparticle interference (see [30]).

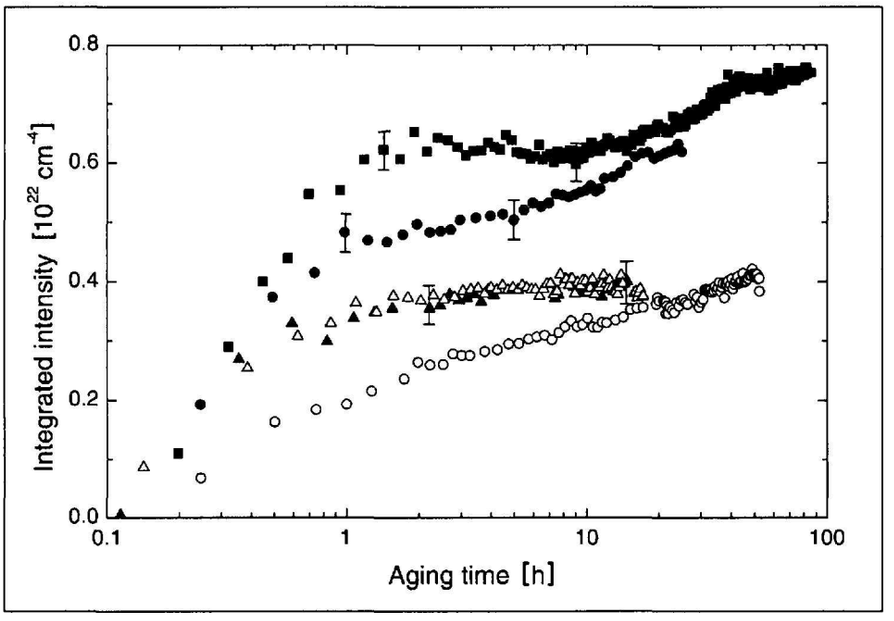

Fig. 6. Integrated SANS intensity as a function of aging time for Ni-11.3 at.% Ti aged at 870 K (filled squares), 900 K (filled circles) and 950 K (full triangles), for Ni-11.1 at.% Ti at 950 K (open triangles) and for Ni-10.1 at.% Ti at 900 K (open circles).

3.2. *Some Results for Ni Alloys*

Ni-based alloys are widely used in structural applications owing to their good mechanical properties and their resistance to corrosion. Ni superalloys in particular exhibit high mechanical strength at elevated temperatures owing to the presence of an ordered phase of hard, coherent precipitates ($L1_2$ structure) embedded in the disordered Ni-rich matrix. Although the technological development of superalloys is quite advanced, there is still a general need to better understand the basic physical processes controlling microstructural changes and the (meta-)stability of decomposed states. In a recent study, small-angle neutron scattering (SANS) has been employed to investigate decomposition in Ni-Ti. The scattering contrast is particularly favourable in this system, as the scattering length of Ti is negative for neutrons.

The complex decomposition sequence in Ni-rich Ni-Ti is of special interest, as metastable states appear during phase separation, whereas the stable ordered η-phase (Ni_3Ti, hexagonal) is observed only after extended aging above about 1200 K. Earlier SANS studies indicated that the metastable states may involve two successive regimes with Ti concentrations of about 18 and 22 at.% (γ'' and γ') [31][32]. These conclusions were drawn from integrated SANS intensities obtained from several samples aged at 850 K for various times and quenched to room temperature. The integrated intensity $\tilde{I}$ is given by

$$\tilde{I} = \int S(\mathbf{Q})d^3\mathbf{Q} = (2\pi)|\rho(\mathbf{r}) - \rho|^2 \quad (13)$$

where the integration includes all $\mathbf{Q}$ values. This requires good quality measurements especially at larger $\mathbf{Q}$, as $S(\mathbf{Q})$ has to be extrapolated for $Q \rightarrow \infty$. In the two-phase model,

$$\tilde{I} = \int S(\mathbf{Q})d^3\mathbf{Q} = (2\pi)|\rho(\mathbf{r}) - \rho|^2 \quad (13)$$

where C_p is the volume fraction of the particles.

Although two regimes can also be distinguished from a scaling analysis of the scattering curves [32], *in situ* studies monitoring the evolution of all stages in the same sample are much more conclusive and have been performed recently. Polycrystals were investigated at SINQ/PSI (Villigen, Switzerland), while single crystals were measured at D11/ILL (Grenoble, France). Special furnaces for SANS were constructed and installed. Thus, quick temperature changes and *in*

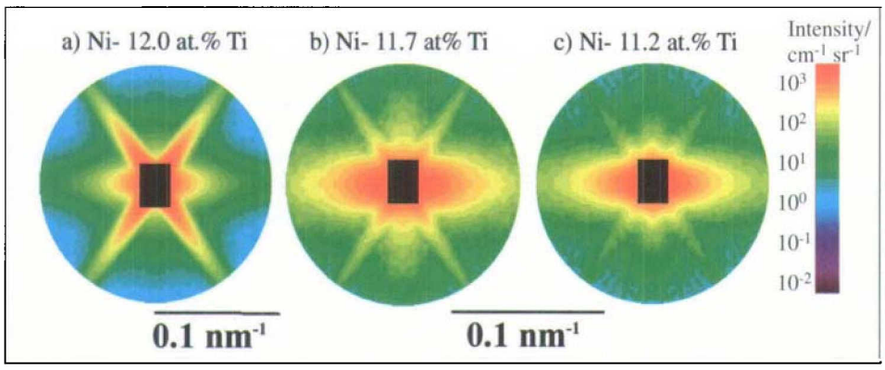

Fig. 7. SANS patterns of Ni-rich Ni-Ti single crystals solution treated at 1440 K and annealed *in situ* for (a) 46 min at 1240 K, (b) 10 min at 1220 K, (c) 43 min at 1200 K. The patterns were symmetrized to highlight the dominating features. The incident beam was parallel to the ⟨110⟩ surface normal of the sample, the horizontal axis is along ⟨100⟩.

situ solid solution treatments at high temperatures became feasible. The homogeneity of any sample can now be directly controlled *via* the SANS intensity by means of the 'flatness' of the scattering patterns.

Polycrystals of Ni-10.1, 11.1 and 11.3 at.% Ti were solution-treated at 1440 K, quenched in water and aged between 870 and 950 K for up to 90 h. The scattering intensity increases with time and shows an interference peak that reflects the alignment of the coherent metastable precipitates along ⟨100⟩. With increasing aging time, the peak position continuously shifts to smaller values of the modulus of the scattering vector. The integrated SANS intensities *vs.* aging time are shown for all polycrystalline samples in Fig. 6. The error is estimated considering the statistical uncertainties of the measured data. An intermediate plateau is clearly visible for Ni-11.3 at.% Ti aged at 870 K after about 2 h, and at 900 K after about 1 h. For Ni-10.1 at.% Ti aged at 900 K for 52 h, no plateau was reached. For the two crystals aged at 950 K a plateau is resolved after about 3 h, but no increase is recorded during the experiment.

The values of Ti content in the precipitates are calculated from the integrated intensity using the Ti content of the matrix from the coherent solvus given by Rastogi and Ardell [33]. The data are in good agreement with the metastable miscibility gap suggested by Hashimoto and Tsujimoto [34]. It seems that the first plateau (γ' state) is only well resolved if the initial state of the alloy within the miscibility gap is located below the ordering temperature [35]. This temperature was calculated within a Bragg-Williams model using effective pair interaction parameters recently determined from diffuse neutron scattering [36].

For single crystals at temperatures near and slightly above the suggested miscibility gap, Fig. 7 shows that the metastable states still prevail, as indicated by the strong SANS intensity along ⟨100⟩, and are still present after 1 h. After some time a new feature progressively dominates the scattering pattern. Sharp intensity streaks start growing along the ⟨111⟩ directions. They are due to the formation of platelets of the hexagonal η-phase. The direct formation of the η-phase without a preceding appearance of metastable states was only observed just below the incoherent (stable) solvus line. Transmission electron microscopical investigations are under way to clarify the spatial evolution of the different states.

Acknowledgements

The authors are grateful to their past and present co-workers, especially M. Kompatscher, M.J. Portmann, S.Y. Yu and to B. Demé (ILL Grenoble), J. Kohlbrecher (PSI Villigen) for their fruitful collaboration. This research has been funded in part by the Swiss National Science Foundation.

Received: March 30, 2001

[1] M. v. Laue, W. Friedrich, P. Knipping, *Ann. Physik* **1912**, *41*, 971.
[2] E.O. Wollan, C.G. Shull, *Phys. Rev.* **1948**, *73*, 830.
[3] M.A. Krivoglaz, in 'Theory of X-Ray and Thermal Neutron Scattering from Real Crystals', Ed. S.C. Moss, Plenum Press, New York, **1969**.
[4] A. Guinier, G. Fournet, 'Small Angle Scattering X-Rays', (transl. by C.B. Walker), Wiley, New York, **1955**.
[5] A. Guinier, 'X-Ray Diffraction', (transl. by P. Lorrain and D. Lorrain), Freeman, San Francisco, **1963**.
[6] G. Porod, in ' Small-Angle X-Ray Scattering', Eds. O. Glatter, O. Kratky, Academic Press, London, **1983**, p. 17.
[7] G. Kostorz, in 'Neutron Scattering' (A Treatise on Materials Science and Technology, Vol.15), Ed. G. Kostorz, Academic Press, New York, **1979**, p. 227.
[8] G. Kostorz, in 'Physical Metallurgy', 4th ed, Eds. R.W. Cahn and P. Haasen, Pergamon Press, **1996**, p. 1116.
[9] G. Bauer, 'Neutron Scattering' (A Treatise on Materials Science and Technology, Vol.15), Ed. G. Kostorz, Academic Press, New York, **1979**, p. 291.
[10] T.J. Hicks, in 'Neutron Scattering' (A Treatise on Materials Science and Technology, Vol.15), Ed. G. Kostorz, Academic Press, New York, **1979**, p. 337.
[11] J.M. Cowley, *J. Appl. Phys.* **1950**, *21*, 24.
[12] L.H. Schwartz, J.B. Cohen, 'Diffraction from Materials', 2nd ed., Springer, Berlin, **1987**.
[13] P.C. Gehlen, J.B. Cohen, *Phys. Rev.* **1965**, *A139*, 844.
[14] S.Y. Yu, B. Schönfeld, G. Kostorz, *Phys. Rev. B* **1997**, *56*, 8535.
[15] P.C. Clapp, *Phys. Rev.* **1971**, *B4*, 255.
[16] F. Ducastelle, in 'Order and Phase Stability in Alloys', North-Holland, Amsterdam, **1991**.
[17] M.D. Asta, D.D. Johnson, *Comput. Mater. Sci.* **1997**, *8*, 64.
[18] V. Gerold, J. Kern, *Acta Metall.* **1987**, *35*, 393.
[19] A.R. Büchner, W. Pitsch, *Z. Metallkd.* **1985**, *76*, 651.
[20] P. Schwander, B. Schönfeld, G. Kostorz, *Phys. Stat. Sol. (b)* **1992**, *172*, 73.
[21] V. Gerold, H.P. Karnthaler, *Acta Metall.* **1989**, *37*, 2177.
[22] H. Roelofs, B. Schönfeld, G. Kostorz, W. Bührer, *Phys. Stat. Sol. (b)* **1995**, *187*, 31.
[23] G. Kostorz, in, 'Non Linear Phenomena in Materials Science III, Solid State Phenomena', Eds. A. Ananthakrishna, L.P. Kubin, G. Martin, vol. 42-43, Scitec Publications Ltd., **1995**, p. 187.
[24] S.I. Hong, C. Laird, *Mater. Sci. Eng.* **1990**, *A124*, 183.
[25] B. Schönfeld, H. Roelofs, A. Malik, G. Kostorz, J. Plessing, H. Neuhäuser, *Acta Mater.* **1996**, *44*, 335.
[26] L. Reinhard, B. Schönfeld, G. Kostorz, W. Bührer, *Phys. Rev.* **1990**, *B41*, 1727.
[27] B. Schönfeld, *Progr. Mater. Sci.* **1999**, *44*, 435.
[28] W.W. Beeman, P. Kaesberg, J.W. Anderegg, M.B. Webb, in 'Handbuch der Physik', vol. 32, Ed. S. Flügge, Springer, Berlin, **1957**, 321.
[29] J.S. Pedersen, *J. Appl. Crystallogr.* **1994**, *27*, 595.
[30] A.D. Sequeira, H.A. Calderon, G. Kostorz, J.S. Pedersen, *Acta Metall. Mater.* **1995**, *43*, 3427.
[31] A. Cerri, B. Schönfeld, G. Kostorz, *Phys. Rev.* **1990**, *B42*, 958.
[32] P. Vyskocil, J.S. Pedersen, G. Kostorz, B. Schönfeld, *Acta Mater.* **1997**, *45*, 3311.
[33] P.K. Rastogi, A.J. Ardell, *Acta Metall.* 1969, *17*, 595.
[34] K. Hashimoto, T. Tsujimoto, *Trans. JIM* **1978**, *19*, 77.
[35] W.A. Soffa, D.E. Laughlin, *Acta Metall.* **1989**, *37*, 3019.
[36] R. Bucher, B. Schönfeld, G. Kostorz, M. Zolliker, *Phys. Stat. Sol. (a)* **1999**, *175*, 527.